

14

Fluorescence Biosensors Utilizing Grating-Assisted Plasmonic Amplification

Koji Toma¹, Mana Toma², Martin Bauch³, Simone Hageneder⁴, and Jakub Dostalek⁴

¹ Department of Biomedical Devices and Instrumentation, Institute of Biomaterials and Bioengineering, Tokyo Medical and Dental University, Tokyo, Japan

² Department of Applied Chemistry for Environment, School of Science and Technology, Kwasei Gakuin University, Sanda, Japan

³ Energy Department, AIT—Austrian Institute of Technology, Vienna, Austria

⁴ Biosensor Technologies, AIT—Austrian Institute of Technology, Vienna, Austria

14.1 Introduction

Fluorescence represents arguably the most-spread analytical method for detection and interaction analysis of biomolecules in important areas of life sciences, medicine, and food safety [1, 2]. The performance characteristics of currently used fluorescence analytical technologies can be tremendously advanced by plasmonic-based manipulation of light. Plasmonics emerged as a novel branch of nanophotonics that focuses on the control of propagation and interaction of light at visible and near infrared part of spectrum by its subwavelength confinement [3, 4]. This confinement occurs due to the excitation of surface plasmons (SPs) originating from collective oscillations of charge density and associated electromagnetic field at surfaces of metallic films and metallic nanostructures. The excitation of SPs is accompanied with strongly enhanced field intensity and local density of states (LDOS) which makes them ideally suited for coupling with fluorescence emitters such as organic dyes and quantum dots. The coupling of fluorophores with the confined field of SPs at their absorption (λ_{ab}) and emission (λ_{em}) wavelengths enables enhancing their “brightness.” In fluorescence bioassays, fluorophores are used as labels for the measurement of specific capturing of target analyte on a sensor surface with immobilized biomolecular recognition elements such as antibodies [5, 6]. The plasmonic amplification of fluorescence light intensity emitted by these labels allows the analysis of smaller number of target molecules on the surface. This can translate to increased sensitivity and improved limit of detection (LOD) of bioassays and thus open doors for the analysis of trace amounts of biomolecules present in analyzed samples. Such

performance is urgently needed in numerous fields including biomarker analysis for early cancer diagnosis and detection of harmful compounds in food.

This chapter deals with surface plasmon-coupled fluorescence emission (SPCE) and its implementations to plasmonically amplified bioassays that utilize diffractive and nondiffractive grating structures. The chapter provides a brief introduction to SPCE relying on reverse Kretschmann configuration and diffraction gratings (Section 14.2) and it discusses the impact of losses of SPs in SPCE studies (Section 14.3), control of SPCE by changing SP dispersion relation by nondiffractive gratings (Section 14.4), extraction of fluorescence light trapped with SPs by diffractive gratings (Section 14.5), and finally it illustrates how these optical phenomena can be employed in fluorescence biosensors for detection of protein analyte (Section 14.6). It should be noted that the chapter does not present a complete review of this field. Rather, it contains a series of examples that were preferably selected from our laboratory and that illustrate recent efforts in the rapidly developing area of plasmonically enhanced fluorescence bioassays.

14.2 SPCE in Vicinity to Metallic Surface

SPs are optical waves at an interface between metal and dielectric that originate from collective oscillations of electron density and associated electromagnetic field. As illustrated in Figure 14.1a, they travel along the interface and their field exponentially decays into both media. The propagation constant of SPs can be expressed as

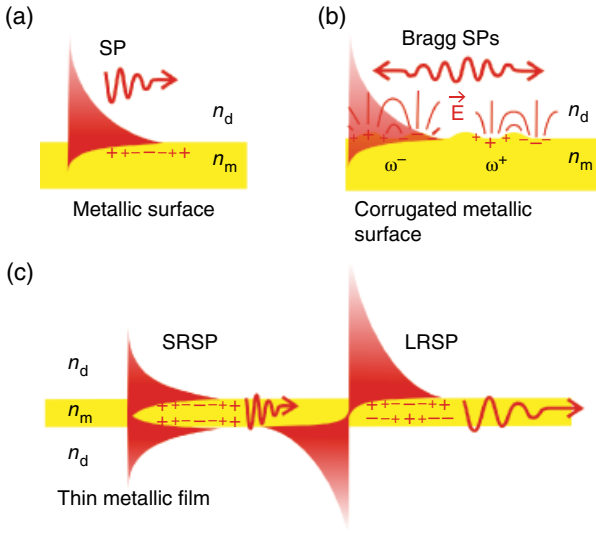


Figure 14.1 (a) SPs traveling along a flat metallic surface, (b) Bragg-scattered SPs on periodically corrugated metallic surface, and (c) long- and short-range SPs on a thin metallic film.

$$k_{\text{SP}} = \frac{2\pi}{\lambda} \sqrt{\frac{n_m^2 n_d^2}{n_m^2 + n_d^2}}, \quad (14.1)$$

where λ states for wavelength, n_m is the refractive index of the metal, and n_d is the refractive index of the dielectric. The real part of the propagation constant $\text{Re}\{k_{\text{SP}}\}$ represents the momentum of SP and the imaginary part $\text{Im}\{k_{\text{SP}}\}$ states for losses of SP due to Ohmic dissipation in the metal. The key characteristics of SPs including the profile of field, dispersion relation, and losses mainly depend on the choice of the SPR-active metal. However, these properties can also be efficiently tuned by using plasmonic structures where multiple SPs couple. For instance, sub-wavelength periodic corrugation of metallic surface allows for diffraction coupling of counter propagating SPs which leads to opening of a bandgap in SP dispersion relation [7]. This scattering occurs for the corrugation period Λ that fulfills the phase matching condition $2\pi/\Lambda = 2\text{Re}\{k_{\text{SP}}\}$. At edges of the induced bandgap, two new Bragg-scattered surface plasmon (BSSP) modes occur as shown in Figure 14.1b. They exhibit standing wave field profile that is weaker confined at the surface and less damped (mode marked as ω^+) or stronger confined at the surface and more damped (mode marked as ω^-).

Another means for tuning the characteristics of SPs provides the near-field coupling of SPs on a thin metallic film, see Figure 14.1c. When such thin metallic film is sandwiched between two dielectrics with similar refractive index n_d , SPs propagating at its bottom and top interfaces interact via their evanescent

tails that penetrate through the metal film. This interaction leads to the occurrence of new modes with symmetric and antisymmetric profile of field [8]. The mode with antisymmetric distribution of electric field intensity E_{\parallel} (component parallel to the surface) is referred as to long-range surface plasmon (LRSP). This mode exhibits smaller losses and less confined field compared to those of regular SPs. The complementary mode to LRSPs exhibits symmetric distribution of E_{\parallel} and it is named short-range surface plasmon (SRSP). Its propagation is more damped and field is stronger confined at the metal surface with respect to regular SPs.

Studies of SP-mediated fluorescence date back to 1970s of the last century when luminescence intensity and lifetime of an emitter in vicinity to metallic surfaces were investigated [9, 10]. At distances between an emitter and metal surface d that are below Förster radius, quenching of fluorescence occurs due to dipole–dipole interaction with electrons in the metal. At longer distances that are comparable with penetration depth of SP field into the adjacent dielectric, strong emission via SPs can be observed. As illustrated by simulations in Figure 14.2a, fluorescence emission is strongly quenched at distances $d < 15$ nm (simulations are presented for randomly oriented emitter at gold–water interface with an emission wavelength of $\lambda_{\text{em}} = 670$ nm). At distances $d \sim 15$ –50 nm, the majority of energy is emitted via SPs. The emission to optical waves propagating into the far field occurs at distances that are further away from the metal $d > 50$ nm and lie outside the SP evanescent field.

Let us note that the majority of fluorescence assays rely on the sandwich detection format using antibodies or antigens for sensing. Antibodies are attached to a solid surface in order to selectively bind target analytes in a sample followed by the binding of detection antibodies that are labeled with a fluorophore, see Figure 14.2b. In such assays, the distance between a fluorophore label and the surface is typically $d = 15$ –20 nm when taking into account the size of immunoglobulin G (IgG) antibodies and that of medium-sized protein analytes [11]. Such distance excellently matches the range where strong coupling between fluorescence emission and SPs occurs, see Figure 14.2a.

Photons that are emitted at λ_{em} via SPs from flat interface between semiinfinite metal and dielectric are dissipated due to Ohmic losses. However, the majority of such fluorescence intensity can be recovered by using couplers based on reverse Kretschmann geometry of attenuated total reflection (ATR) method [5, 12, 13] or diffraction on periodically corrugated metal surface [14, 15]. These techniques allow for extracting the emitted fluorescence light

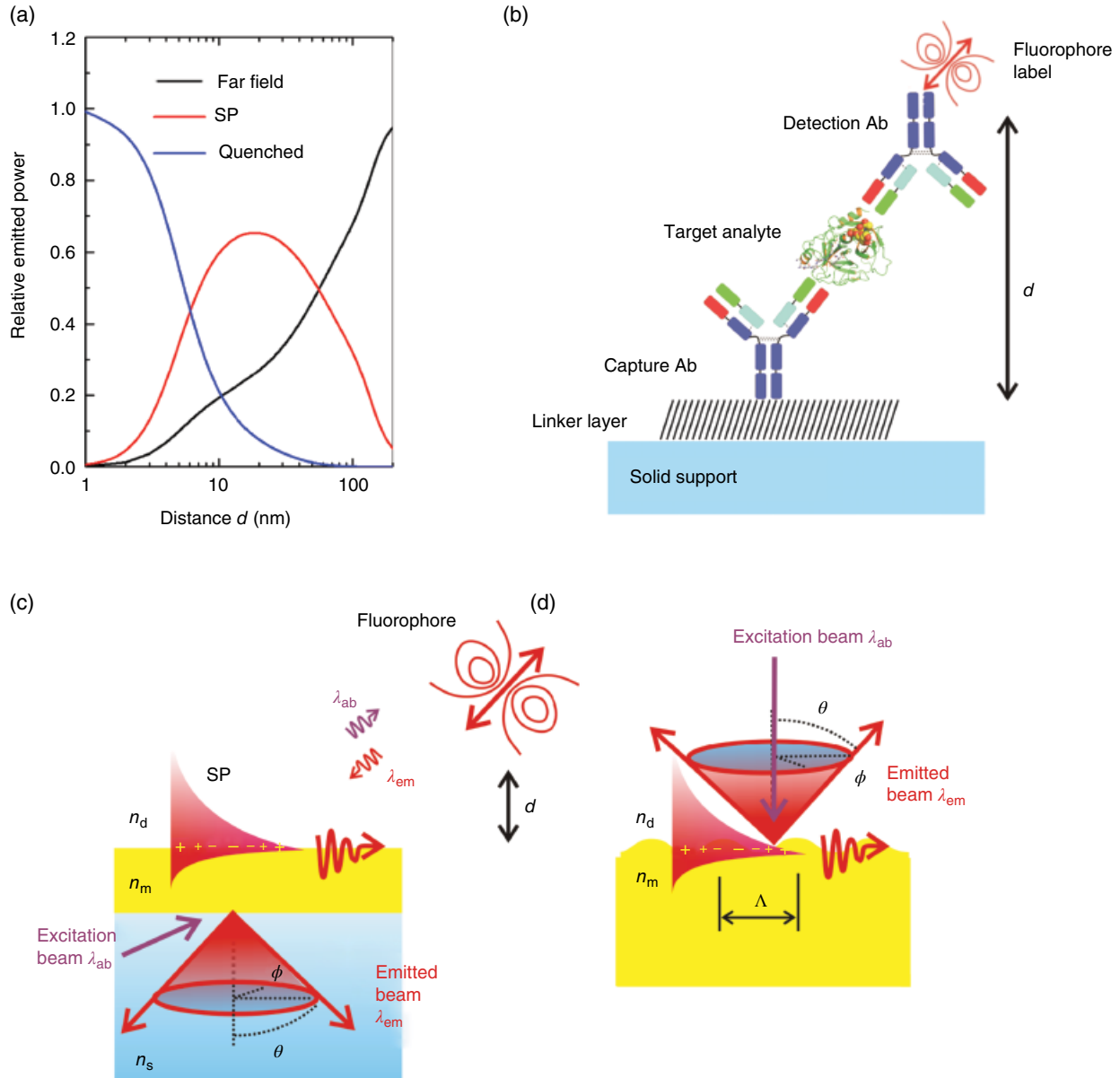


Figure 14.2 (a) Distance dependence of relative power radiated by randomly oriented emitter from a flat gold–water interface at $\lambda_{em} = 670$ nm that is quenched, coupled to SPs, and emitted to the far field. (b) Schematics of sandwich immunoassay utilizing fluorophore labels. Geometry used for out-coupling of SP modes via, (c) reverse Kretschmann geometry of ATR method and (d) by using diffraction on periodically corrugated metallic surface. (See insert for color representation of this figure.)

that are trapped by SPs to a highly directional fluorescence beam propagating to the far field. In the reverse Kretschmann configuration depicted in Figure 14.2c, the SPs propagating on a thin metallic film leak into a dielectric substrate with high refractive index n_s . This leakage occurs for narrow range of polar angles θ for which the light beam propagating in the high refractive index dielectric is phase-matched with SPs propagating along the upper interface between the metal and a dielectric with low refractive index n_d .

$$\frac{2\pi}{\lambda} n_s \sin(\theta) = \text{Re}\{k_{SP}\}. \quad (14.2)$$

It should be noted that SPs preferably collect fluorescence light that originates from emitters with emission dipole oriented perpendicular to the surface. The reason is that SP field is transverse magnetically (TM) polarized and its strongest component of electric intensity vector is oriented normal to the surface. For an ensemble of randomly oriented emitters, emission is averaged over the azimuthal angle ϕ and the SPCE

beam in the dielectric substrate with the high index of refraction n_s exhibits a characteristic cone shape defined by the (resonant) polar angle θ .

An alternative means for extracting of fluorescence light energy stored in SPs relies on periodically corrugated interface between a metallic and dielectric (see Figure 14.2d). Diffraction on the periodic corrugation allows for converting SPs to the far field by the grating momentum $G = 2\pi/\Lambda$. This momentum couples the SP-driven emission to an optical wave propagating away from the surface with the polar angle θ and azimuthal angle ϕ that fulfill the following condition:

$$\frac{2\pi}{\lambda} n_d \sin(\theta) \cos(\phi) + m \frac{2\pi}{\Lambda} = \pm \text{Re}\{k_{\text{SP}}\}, \quad (14.3)$$

where Λ is the period of the corrugating with the grating vector G oriented in the direction $\phi = 0$.

Besides the coupling of fluorescence emitters with SPs at emission wavelength λ_{em} , the confined SP field can also interact with a fluorophore at its absorption wavelength λ_{ab} . The resonant excitation of SPs generates enhanced field intensity $|E/E_0|^2$ in close vicinity to metallic surface. At λ_{ab} , this field can increase the excitation rate of emitters γ_e which is proportional to the emitted fluorescence signal F when it is far from saturation. In optical instruments supporting fluorescence biosensors, plasmonically increased excitation rate γ_e and controlled angular distribution of emitted fluorescence light $F(\theta, \phi)$ can be preferably combined. These features allow to maximize detected fluorescence signal that originates from the molecular binding at the surface and to minimize parasitic background. The overall enhancement factor of detected fluorescence light intensity EF can be expressed as a product.

$$\text{EF} \propto \left| \frac{E}{E_0} \right|^2 \times \frac{\eta}{\eta_0} \times f, \quad (14.4)$$

Here, η states the quantum yield of the emitter coupled to SPs on a metallic surface and η_0 is the quantum yield of the emitter far from the metal. The term f states the enhanced probability of collecting emitted photons by plasmonic redistribution of emitted fluorescence intensity $F(\theta, \phi)$.

14.3 SPCE Utilizing SP Waves with Small Losses

Decreasing the angular width of directional SPCE beam is beneficial for various kinds of fluorescence measurements as it, for example, allows to better distinguish the specific fluorescence signal originating

from the close proximity to a metal surface and the (isotropic) background signal. In order to do so, Toma *et al.* [16] employed LRSPs for mediating fluorescence emission from Alexa Fluor 647 emitters dispersed in a three-dimensional (3D) hydrogel matrix, see Figure 14.3a. These SP waves exhibit lower Ohmic losses compared to regular SPs. When using the reverse Kretschmann geometry, the low losses of LRSPs lead to their resonant coupling with the far-field optical waves at narrow range of polar angles θ that fulfill the condition (14.2). For the geometry with a 19-nm thick gold film deposited on a low refractive index Cytop layer with the thickness of 650 nm, LRSPs provided 4.4-fold higher peak fluorescence intensity and 6-fold narrower full width at half maximum (FWHM) than those of regular SPs when both excitation (at λ_{ab}) and collection of fluorescence light (at λ_{em}) were mediated by SP waves, see Figure 14.3b. The emitters dispersed in the 3D hydrogel matrix were efficiently probed by LRSP field which exhibits less localized field profile, that is, penetrating deeper from the metal film than regular SPs. The average electric field intensity enhancement within 600-nm thick hydrogel film was of $|E/E_0|^2 = 37$ upon the resonant excitation of LRSPs at the wavelength 633 nm, while for regular SPs it was only about 8. In addition, Figure 14.3b shows that LRSP-mediated SPCE occurs at smaller polar angle θ , which, together with the narrower angular distribution, can simplify optics for collecting of SPCE as a smaller numerical aperture (NA) lens can be used.

A recently emerged alternative to SPs for fluorescence enhancement is based on dielectric one-dimensional photonic crystals (1DPC) [17, 18]. These structures can be designed to support the so-called Bloch surface waves (BSWs) that exhibit similar properties to SPs and offer the advantage of versatile tunability. In addition, as the 1DPC comprises a stack of alternating dielectric layers, the losses of BSW are dramatically lower compared to those of SP-based structures. In the work of Toma *et al.* [19], BSWs were employed for the excitation of Alexa Fluor 647 dyes on the surface of a fluorescence biosensor. The schematic of developed BSW-enhanced fluorescence sensor is shown in Figure 14.4a. It relies on Kretschmann configuration for the coupling of an excitation light beam to BSW that probes the interface covered with a 3D hydrogel binding matrix. This matrix features highly open structure due to its swelling in aqueous samples and thus provides huge surface area for the modification with catcher mouse IgG antibodies. The target molecules (antimouse IgG) labeled with Alexa Fluor 647 were affinity bound in the matrix and excited by BSWs. The emitted

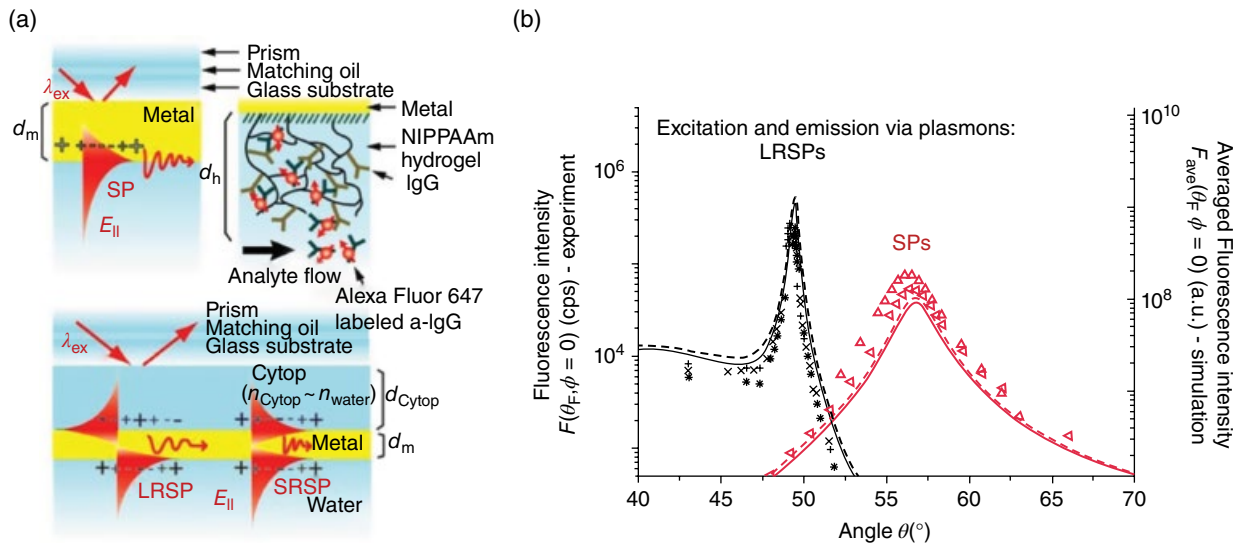


Figure 14.3 (a) Schematic diagrams of the layer architectures for the excitation of regular SPs and LRSPs in order to probe affinity binding of Alexa Fluor 647—labeled antimouse IgG in a 3D hydrogel binding matrix. (b) Angular distribution of SP-coupled emission with (reverse) Kretschmann architecture for the excitation and collection of fluorescence light. Comparison of LRSP and regular SP-coupled emission obtained from experiment (symbols) and simulations (lines) is presented. Toma *et al.* [16]. Reproduced with the permission of The Optical Society.

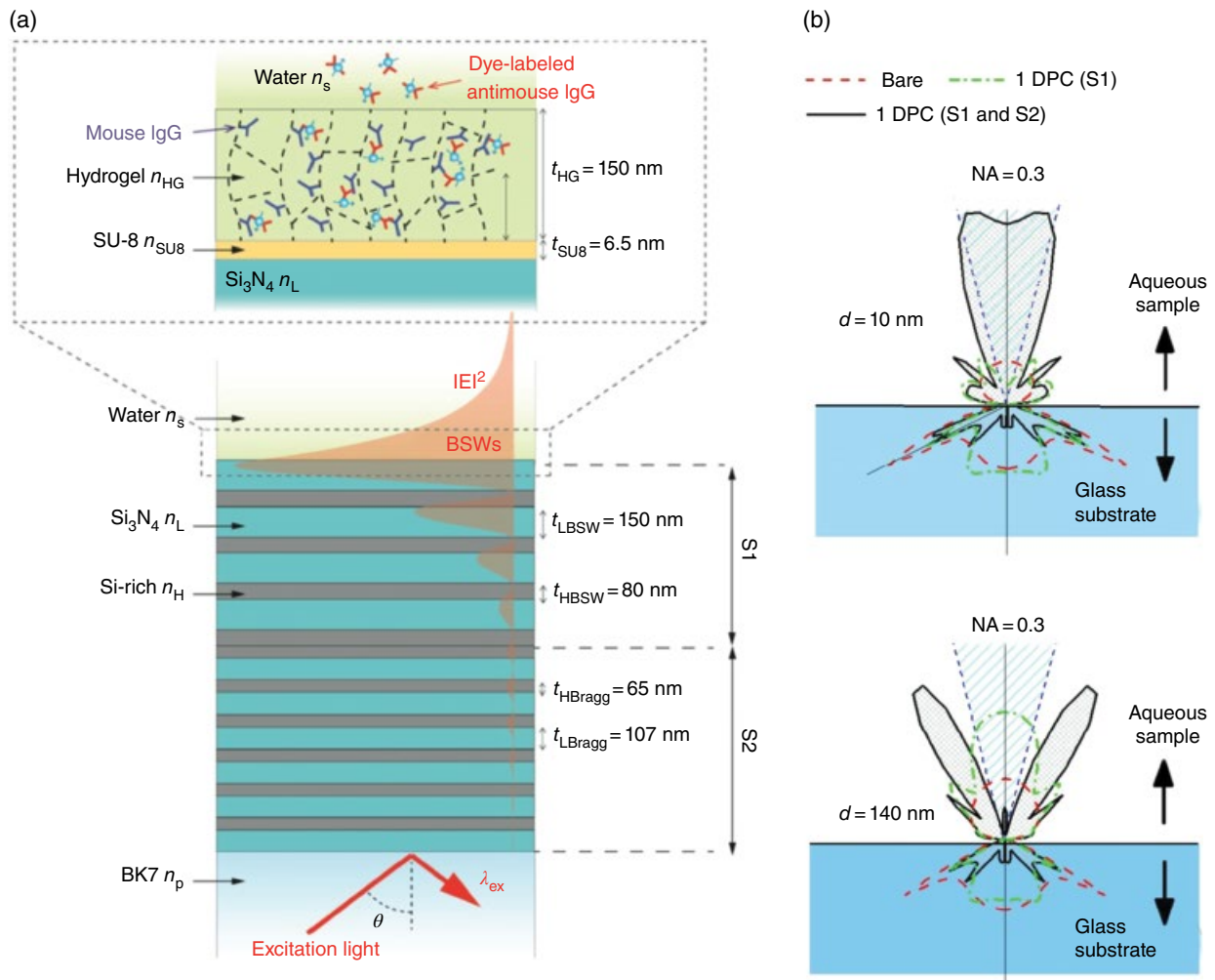


Figure 14.4 (a) Schematics of the surface architecture with periodic stack of dielectric layers that support BSW (S1) and that serves as a Bragg mirror (S2) suppressing the leakage of fluorescence light into the substrate. (b) Simulated angular distribution of emitted light intensity by randomly oriented emitter at the distance from the surface $d = 10$ and 140 nm. Toma *et al.* [19]. Reproduced with the permission of The Optical Society.

fluorescence light was collected with a lens (numerical aperture $NA = 0.3$) through the aqueous sample and a transparent flow cell. The 1DPC was designed so the BSWs were supported only at λ_{ab} , while no BSW existed at the emission wavelength λ_{em} in order to avoid (in this case unwanted) leaking of fluorescence emission into the glass substrate. Due to the minimized losses of BSW, the maximum electric field intensity enhancement accompanied with the resonant excitation of BSWs of as $|E/E_0|^2 = 300$ was simulated (not taking into account the practical losses due to, for example, scattering on the surface roughness). In order to enhance the collection efficiency of emitted fluorescence light through the aqueous sample f , the layer structure comprised two segments: the first segment (S1) served for the resonant excitation of BSWs at λ_{ab} and the second segment (S2) was designed to function as a Bragg mirror at λ_{em} in order to shape the angular distribution of emitted fluorescence light $F(\theta)$. As Figure 14.4b illustrates, Bragg mirror S2 worked not only as a reflector but also provided “beaming” of fluorescence light intensity toward a detector at a water side. The simulated polar angular distribution $F(\theta)$ indicates that the fluorescence light is squeezed in a narrow angular range that matches the acceptance angle of used lens with $NA = 0.3$ for emitters close to the surface. The fluorescence emission probability within this NA reached about 12% for the distance $d = 10$ nm. Since back-reflected fluorescence from 1DPC gains a different phase-shift when changing the distance, the peak intensity occurs at polar angles θ shifted by about 18° when changing d from 10 to 140 nm.

14.4 Nondiffractive Grating Structures for Angular Control of SPCE

Besides structures periodic in the direction perpendicular to the surface, also periodic corrugation in the direction parallel to the surface allows for control of the angular distribution of SPCE that is extracted by reverse Kretschmann configuration. Toma *et al.* explored SPCE mediated by nondiffractive metallic gratings the split of the dispersion relation of SPs by a plasmonic bandgap [20]. In this study, a 50-nm thick Au layer was sinusoidal modulated with a period of $\lambda = 225\text{--}230$ nm and a depth of 10 and 30 nm. The structure was prepared by laser interference lithography and multiple copies were prepared by UV nanoimprint lithography. It was designed for the excitation of BSSPs at edges of the plasmonic bandgap occurring

at wavelengths that coincide with the emission wavelength of DiD fluorophore ($\lambda_{em} = 665$ nm). This fluorophore was dispersed in poly(methyl methacrylate) (PMMA) layer deposited on the top Au layer, see Figure 14.5a. Refractive indices of media below and above the Au layer were tuned in order to adjust wavelength position of the plasmonic bandgap. The dispersion relation of SPs was observed from the measurements of reflectivity spectra as a function of polar angle of incidence θ and wavelength λ taken by the ATR method with Kretschmann geometry. In order to observe the angular distribution of fluorescence intensity $F(\theta, \phi)$ that was mediated by BSSPs, the dye-doped PMMA layer was excited by normally incidence beam with $\lambda = 633$ nm hitting the surface from superstrate side, the fluorescence beam leaking into the underneath glass substrate was scattered by an optically matched diffuser, and imaged to a charge coupled device (CCD).

Figure 14.5b shows several examples of SP dispersion relation mediated by the nondiffractive dense grating and corresponding angular distribution of fluorescence intensity $F(\theta, \phi)$. In part (i), SP dispersion relation and corresponding SPCE angular distribution for a reference flat Au layer structure with air on the top (superstrate refractive index $n_6 = 1$) are presented. A continuous dark band in the reflectivity spectrum $R(\lambda, \theta)$ is due to the excitation of SPs at the outer interface with dye-doped PMMA layer. It reveals that SPR occurs at the angle $\theta \sim 39^\circ$ in the LaSFN9 glass substrate for the emission wavelength $\lambda_{em} = 670$ nm. The respective fluorescence angular distribution $F(\theta, \phi)$ displays a characteristic SPCE cone for the similar polar angle of $\theta \sim 38^\circ$.

When the layer structure is corrugated with the modulation depth of 10 nm and the metal surface is brought in contact with water ($n_6 = 1.33$), the resonant coupling to SPs shifts to higher angles and a plasmonic bandgap appears in the dispersion relation. As seen in Figure 14.5b(ii), BSSP modes occur at wavelengths of $\lambda = 670$ nm (ω^+) and 700 nm (ω^-). Therefore, the BSSP ω^+ wavelength matches the fluorescence emission wavelength λ_{em} of used dye which lead to the confinement of SPCE signal in the direction parallel to grating vector G . Interestingly, the peak emission via BSSP ω^+ mode was increased by a factor of ~ 3 compared to that for regular SPCE cone. The reason is the enhanced LDOS associated with the presence of BSSP. It should be noted that the emission via BSSPs occurs only at narrow range of azimuthal angles ϕ as the bandgap blue shifts away from the emission wavelength λ_{em} by increasing ϕ .

Figure 14.5b(iii) shows the dispersion relation and the corresponding SPCE angular distribution $F(\theta, \phi)$

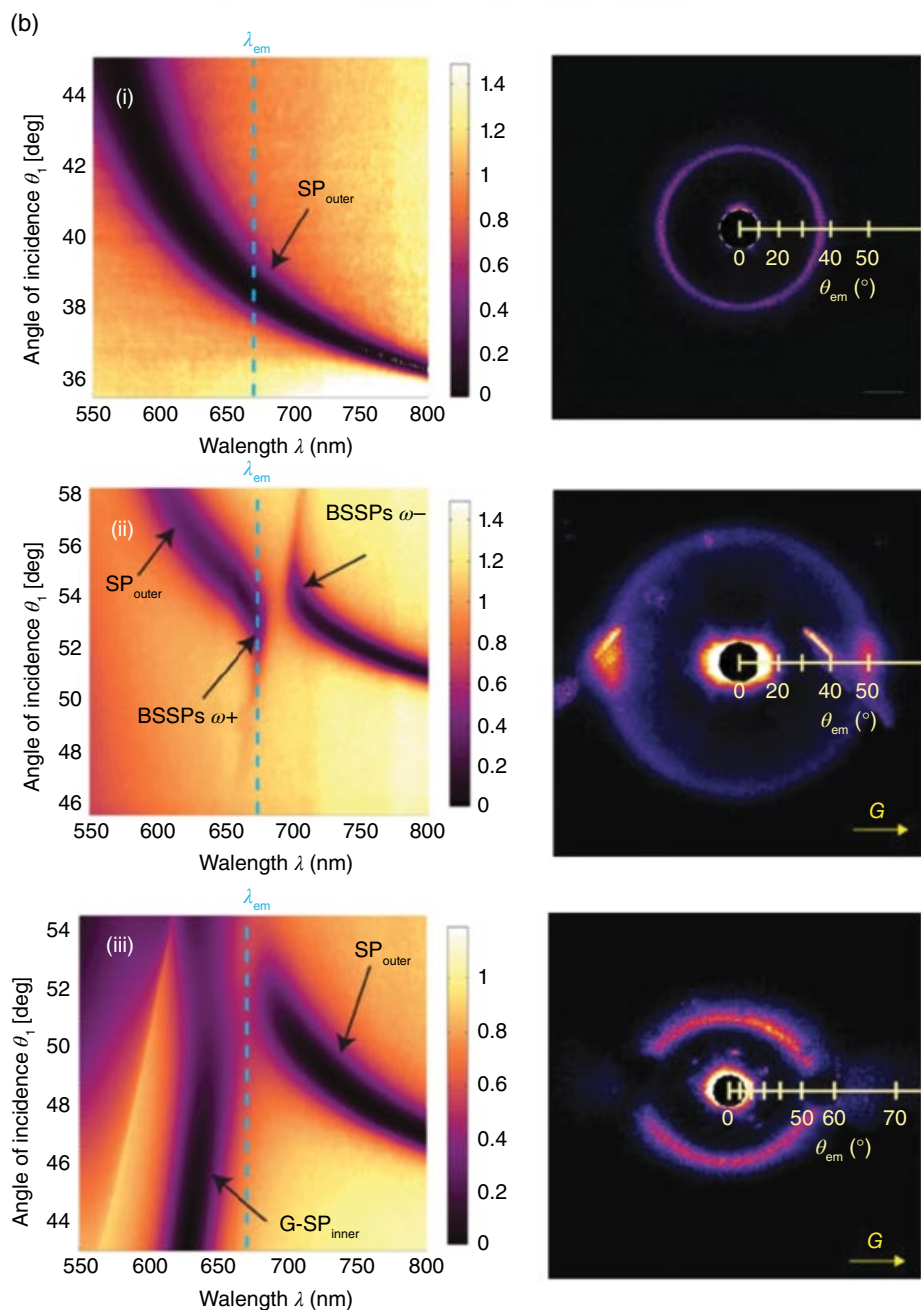
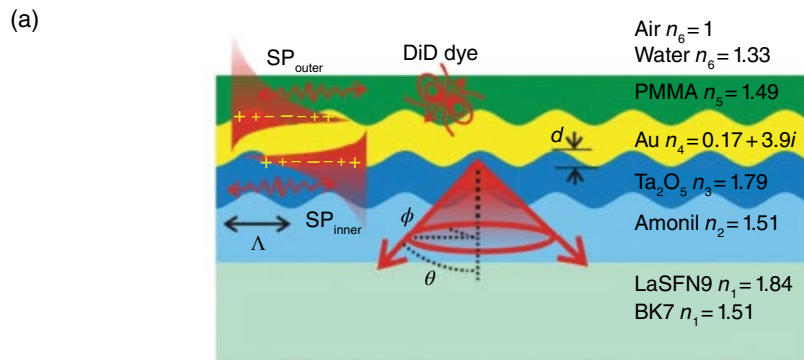


Figure 14.5 (a) Nondiffractive metallic grating structure for probing a thin poly(methyl methacrylate) —PMMA—layer doped with a DiD dye. (b) Examples of SP dispersion relation perturbed by Bragg scattering and respective angular dependence of SPCE $F(\theta, \phi)$ for (i) flat surface, (ii) emission wavelength λ_{em} tuned to the edge of a plasmonic bandgap, and (iii) inside the bandgap. Toma *et al.* [20]. Reproduced with the permission of The Optical Society.

when the grating structure supports SPs that are diffraction coupled across the Au layer. In this experiment, the grating with the modulation depth of 30 nm and without Ta₂O₅ layer was brought into contact with air ($n_6 = 1$). As can be seen from measured data, the dispersion relation of inner SP (that is excited by -1st diffraction order) anticrosses with that of outer SP (excited by ATR and probing the PMMA layer) at the wavelength that coincides with λ_{em} of used DiD dye. Contrary to situation (ii), the anticrossing SP dispersion leads to canceling of the SPCE signal at the direction of parallel with grating vector G .

14.5 Diffractive Grating Structures for Angular Control of SPCE

On periodically corrugated metallic surfaces with longer periods Λ , diffraction allows to directly extract fluorescence light emitted via SPs into the far field (see Eq. (14.3)). Bauch *et al.* [21] investigated grating-enhanced fluorescence on crossed periodically corrugated Au surface that is depicted in Figure 14.6a. This structure has been designed to resonantly excite SPs by normally incident laser beam with wavelength λ_{ab} and to diffractively out-couple SPCE at λ_{em} into a narrow emission cone traveling back into direction of the

incident excitation beam. Such a design is attractive for the use in fluorescence sensors relying on epifluorescence geometry that is implemented in the majority of fluorescence microarray scanners and fluorescence microscopes [22]. The used structure comprised two superimposed sinusoidal modulations orientated at 90° to each other. It was prepared by laser interference lithography and multiple copies were made by UV nanoimprint lithography which is compatible with mass production technologies. The grating structure was optimized for the amplification of *in situ* fluorescence sandwich immunoassays with Cy5 and Alexa Fluor 647 dyes when the excitation wavelength $\lambda = 633$ nm and the emission is centered at the wavelength $\lambda_{em} = 670$ nm. The grating period was of $\Lambda = 434$ nm and the surface was coated with 4-nm thick adhesion promoting Cr layer and optically thick 100-nm Au film.

Contrary to the Kretschmann configuration, diffraction coupling to SPs on a crossed grating leads to the amplified electric field intensity that varies in lateral direction. The averaged electric field intensity enhancement $|E/E_0|^2$ generated by the resonant excitation of SPs at λ_{ab} is compared with that on a flat Au surface in Figure 14.6b. On a crossed grating, maximum field intensity occurs at the interface between Au and aqueous sample and it exponentially decays into both metal and water media. On a flat surface, the field exhibits minimum intensity at the Au surface and it oscillates when increasing the

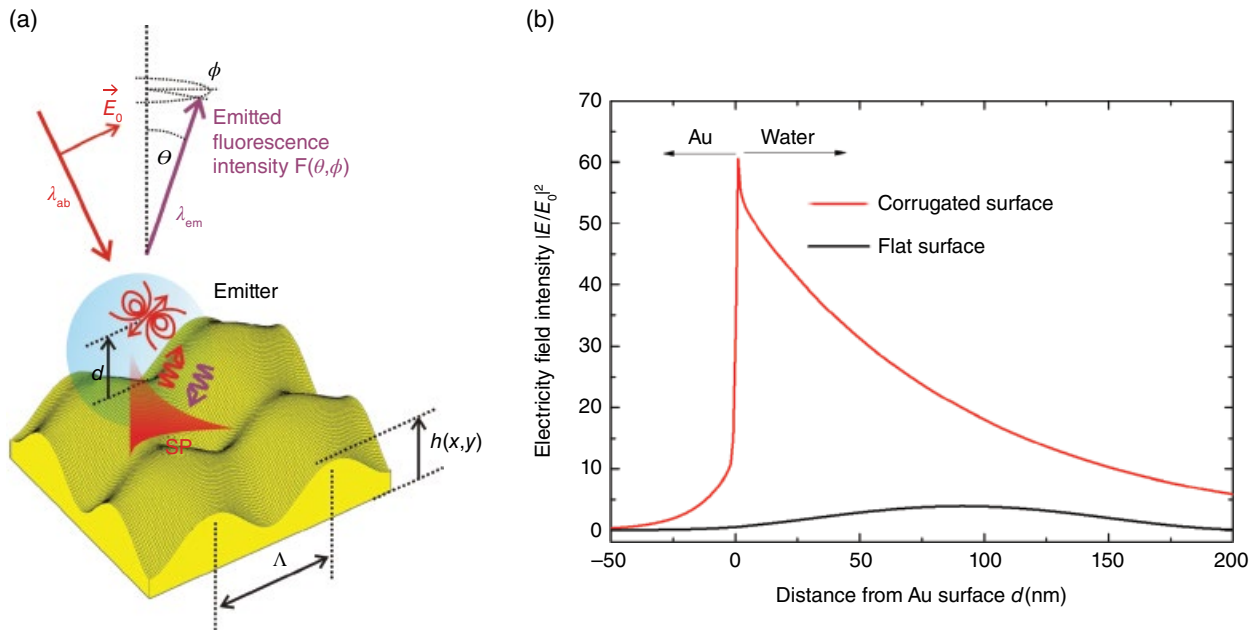


Figure 14.6 (a) Geometry and (b) electric field intensity $|E/E_0|^2$ averaged over the unit cell of the diffractive grating upon the resonant diffractive coupling to SPs. The field strength was calculated as a function of distance d from the flat and corrugated gold surfaces. Normally, incident plane wave at the wavelength of $\lambda_{ab} = 633$ nm was assumed. Bauch *et al.* [21]. Reproduced with the permission of The Optical Society.

distance d due to the interference of the incident and reflected beams. The electric field intensity at a distance of $d=20$ nm that is normalized with the intensity of the incident beam is around $|E/E_0|^2=43$ for the resonant coupling to SPs on the corrugated surface. The simulated data on a flat Au surface show much lower field strength $|E/E_0|^2=1.36$ at such distance d .

After its excitation, a fluorophore decays back to its ground state by radiative or nonradiative processes. The vicinity of metal alters both the radiative and nonradiative decay rates and therefore changes the quantum yield of the fluorophore η [23]. It should be noted that plasmonic nanostructures have been reported to significantly increase quantum yield of emitters with low intrinsic quantum yield η_0 [24]. However, for the assay that utilizes relatively high intrinsic quantum yield fluorophore Alexa Fluor 647 ($\eta_0=0.33$), this effect is weak and rather a small decrease in quantum yield occurs $\eta/\eta_0=0.82$. Therefore, mostly the first term $|E/E_0|^2$ and last term f in Eq. (14.4) play important role for maximizing fluorescence assay sensitivity.

The grating-coupled emission of fluorescence light enables controlling the angular distribution of emitted light intensity $F(\theta,\phi)$ at λ_{em} in order to improve fluorescence collection efficiency f . As shown by

simulated data in Figure 14.7a, the emission angular distribution $F(\theta,\phi)$ at the flat gold surface is isotropic while that on crossed grating displays series of bright bands due to the first-order diffraction out-coupling of SPCE. These bands lead to a confinement of emitted fluorescence light energy in a narrow cone of polar angles $\theta < 11.5^\circ$ which allows for efficient collecting of fluorescence light by a low numerical aperture lens with $NA=0.2$. These simulations predicted that the interplay of plasmonically increased excitation rate by $|E/E_0|^2$ at λ_{ab} , modified quantum yield η/η_0 , and increased collection efficiency f at λ_{em} allows to increase fluorescence signal on a crossed Au grating with respect to flat Au surface by a factor $EF=145$ for $d=15$ nm and $EF=96$ for $d=20$ nm.

Figure 14.7b confirms predicted simulations by measurements of fluorescence far-field emission $F(\theta,\phi)$. These measurements were carried out for DiD dye dispersed in a thin PMMA layer deposited on a flat and corrugated Au surfaces. The DiD dye exhibits similar absorption and emission spectra as Alexa Fluor 647 and Cy5 employed in bioassays. The observed behavior qualitatively agrees with the simulated data in Figure 14.7a. The emission bands are broader than those predicted by simulations due to the fact that the emitted light within a spectral range $\lambda_{em} \sim 665\text{--}675$ nm was collected and imaged to the detector.

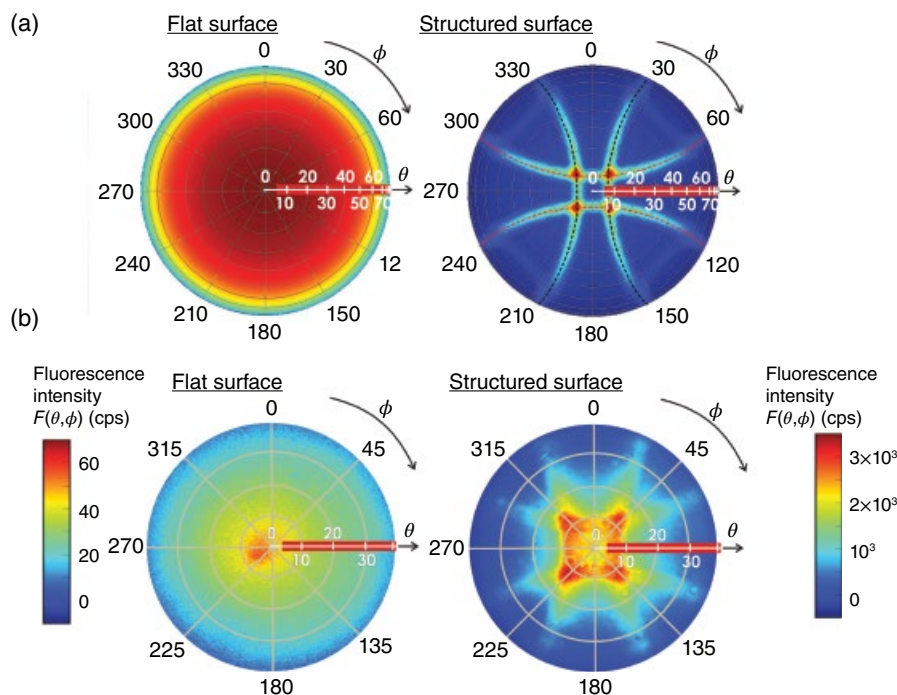


Figure 14.7 (a) Simulated and (b) measured angular distribution of far-field fluorescence intensity $F(\theta,\phi)$ emitted from randomly oriented DiD dyes dispersed in a poly (methyl methacrylate) layer that was prepared on a flat (left) and corrugated (right) Au surfaces. The polar angle θ is given in air. Bauch *et al.* [21]. Reproduced with the permission of The Optical Society.

14.6 Implementation of Grating-Assisted SPCE to Biosensors

Bauch *et al.* demonstrated that designed diffractive grating provides enhanced fluorescence signal by a factor $EF \sim 10^2$ when applied for an immunoassay detection with *in situ* format and epifluorescence readout geometry. As sketched in Figure 14.8a, an optical instrument with a grating sensor chip clamped to a microfluidic device was used for the measurement of affinity binding of biomolecules at the sensor surface. The sensor chip was functionalized with antibodies for specific capture of the medium-sized protein interleukin 6 (IL6) that has been established as an inflammatory biomarker. Detection antibody (dAb) labeled with Alexa Fluor 647 was bound to the captured IL6 in the used sandwich immunoassays and detected by plasmonically amplified fluorescence. Figure 14.8b shows the kinetics of fluorescence signal F measured upon the affinity binding of dAb. It reveals that the selective amplification of fluorescence signal at the grating surface enables distinguishing the fluorescence signal associated with the binding at the surface from that originating from the bulk solution through which the excitation beam passes. On a flat reference surface, the observed change in fluorescence signal F is mostly due to the bulk and it is manifested as a rapid increase in fluorescence signal after the injecting dAb ($t = 75$ min)

and decrease in fluorescence signal after the rinsing ($t = 85$ min). On the plasmonic grating chip, the relative signal due to the background is massively suppressed and the observed changes in fluorescence signal are virtually attributed only to the analyte bound at the surface that is probed by confined field of SPs.

It should be noted that high numerical aperture optics cannot be easily used for *in situ* epifluorescence measurement when the excitation and collection of fluorescence light are carried out through a microfluidic device. Then, only a low numerical aperture lens can be employed and thus the directional fluorescence emission offers essential advantage of enhanced efficiency in the fluorescence light collection (which otherwise is omnidirectional and only a small fraction of emitted photons are delivered to the detector). However, the majority of currently used fluorescence microarrays scanners are designed for the *ex situ* measurement performed on a dry sensor chip after multiple assay steps. Typically, the excitation beam is scanned over the sensor surface with a high numerical aperture lens that is at the same time used for the collection of fluorescence light. For these optical instruments, the directional SPCE provides limited advantage as the directional emission only redistributes the angular dependence of fluorescence emission within the acceptance cone defined by the maximum polar angle θ_{\max} (see Figure 14.8) [25].

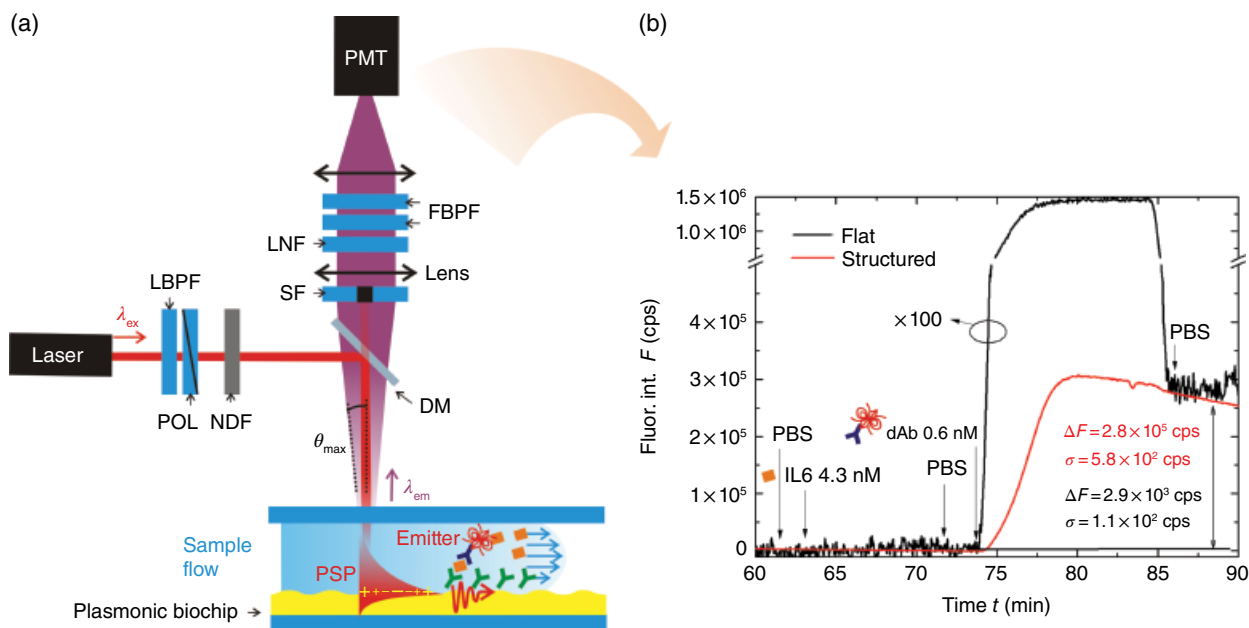


Figure 14.8 (a) Arrangement of an optical instrument for *in situ* fluorescence assay with epifluorescence readout geometry and low numerical aperture lens for the collection of fluorescence light. (b) Example of fluorescence intensity kinetics measured on Au diffraction grating and reference flat Au surface upon the affinity binding of dAb labeled with an Alexa Fluor 647 dye. Bauch *et al.* [21]. Reproduced with the permission of The Optical Society.

Plasmonic biosensor with grating chip for *in situ* sandwich immunoassay detection of inflammation biomarker IL6 was calibrated. In this experiment, a series of buffer samples were spiked with IL6 at concentration c between 10 pg/mL and 100 ng/mL and flown over the sensor chip which carried antibodies against IL6 on its surface. After the IL6 analyte capture, a biotinylated dAb against another epitope of IL6 was injected and bound at the surface. Then, streptavidin labeled with Alexa Fluor 647 was reacted to these biotin moieties, the sensor surface was rinsed with a buffer, and the fluorescence signal difference ΔF before the injection of IL6 analyte and after the streptavidin binding was measured. The whole assay required 50 min including 15-min incubation of the analyzed sample with the capture antibody. Figure 14.9 shows the obtained calibration curves for two assays performed on the structured Au grating chip (gray curve) and a reference flat Au surface (black curve). It demonstrates that plasmonic amplification of fluorescence signal ΔF associated with the capture of IL6 allowed reaching the LOD of 9 pg/mL. This LOD is about 25 times better than that observed on a control flat Au substrate—233 pg/mL. The LOD was determined as an intersection of a linear fit of the measured calibration curve with a background signal ΔF (originating from nonspecific adsorption of labeled streptavidin) plus the 3-fold standard deviation 3σ of measured fluorescence signal. The improvement factor of LOD (25-fold) is lower than the observed EF of the fluorescence intensity (10^2) which is due to the effect of nonspecific adsorption.

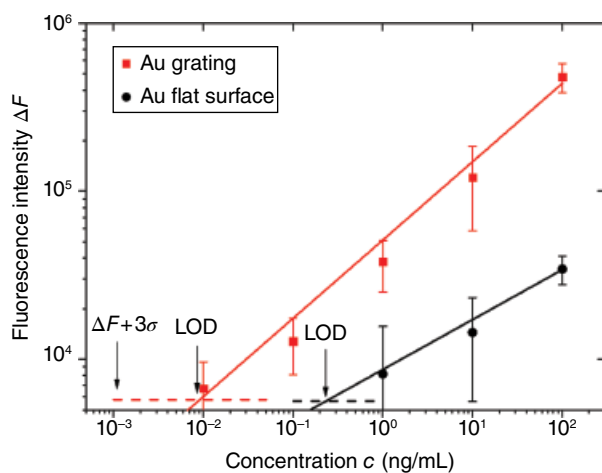


Figure 14.9 Comparison of calibration curves for an IL6 sandwich assay with epifluorescence readout on a structured plasmonic Au surface (gray squares) and a reference flat Au surface (black circles) with corresponding fits and LOD indicated.

As an alternative approach to reverse Kretschmann configuration which typically requires optical matching of a sensor chip to a high refractive index glass prism, Toma *et al.* combined this method with diffractive optical elements [26]. In this work, two gratings were integrated to a compact SPCE sensor chip as depicted in Figure 14.10a. The first one was a linear grating and it served for in-coupling of an excitation light beam to the chip. The excitation beam traveled in the sensor chip and hit the sensing spot at an SP resonance angle for the absorption wavelength of used dye λ_{ab} . The second one was a chirped concentric grating designed for the out-coupling of SPCE cone that propagated in the compact chip. After hitting the concentric grating, the SPCE beam was coupled to -1 st diffraction order that traveled away from the sensor chip and converged to a spot below its bottom surface at a distance $D = 15$ mm, see Figure 14.10b. A flat sensing spot was in the center of the concentric grating and it was coated with a 50-nm thick Au film. At this area, the excitation beam generated SPs at the λ_{ab} in order to enhance excitation rate γ_e of fluorescence light that was subsequently collected by SPs at λ_{em} , leaked into the substrate in the form of SPCE cone, and was imaged to a detector by the concentric grating.

A model immunoassay experiment with such a sensor chip was carried out. As seen in Figure 14.10c, this platform offered comparable sensitivity to regular SP-enhanced fluorescence biosensors relying on Kretschmann configuration with a prism coupler. The compact sensor chip platform with the integrated diffractive elements offers the advantage of simpler design that is attractive for portable fluorescence biosensor devices. The designed elements were prepared by using UV nanoimprint lithography from masters fabricated by laser interference lithography which is compatible with mass production technologies and thus suitable for cost effective fabrication.

14.7 Summary

Several approaches for controlling of SPCE by using diffractive and nondiffractive gratings are described. By this means, the angular distribution of fluorescence light that is emitted from close proximity to a metallic surface can be efficiently tailored for maximizing assay sensitivity. In fluorescence bioassays, this approach enables increasing the detected fluorescence intensity that originates from specific capture of target analyte from a liquid sample at the sensor surface. This amplification allows to better discriminate the specific signal from the background

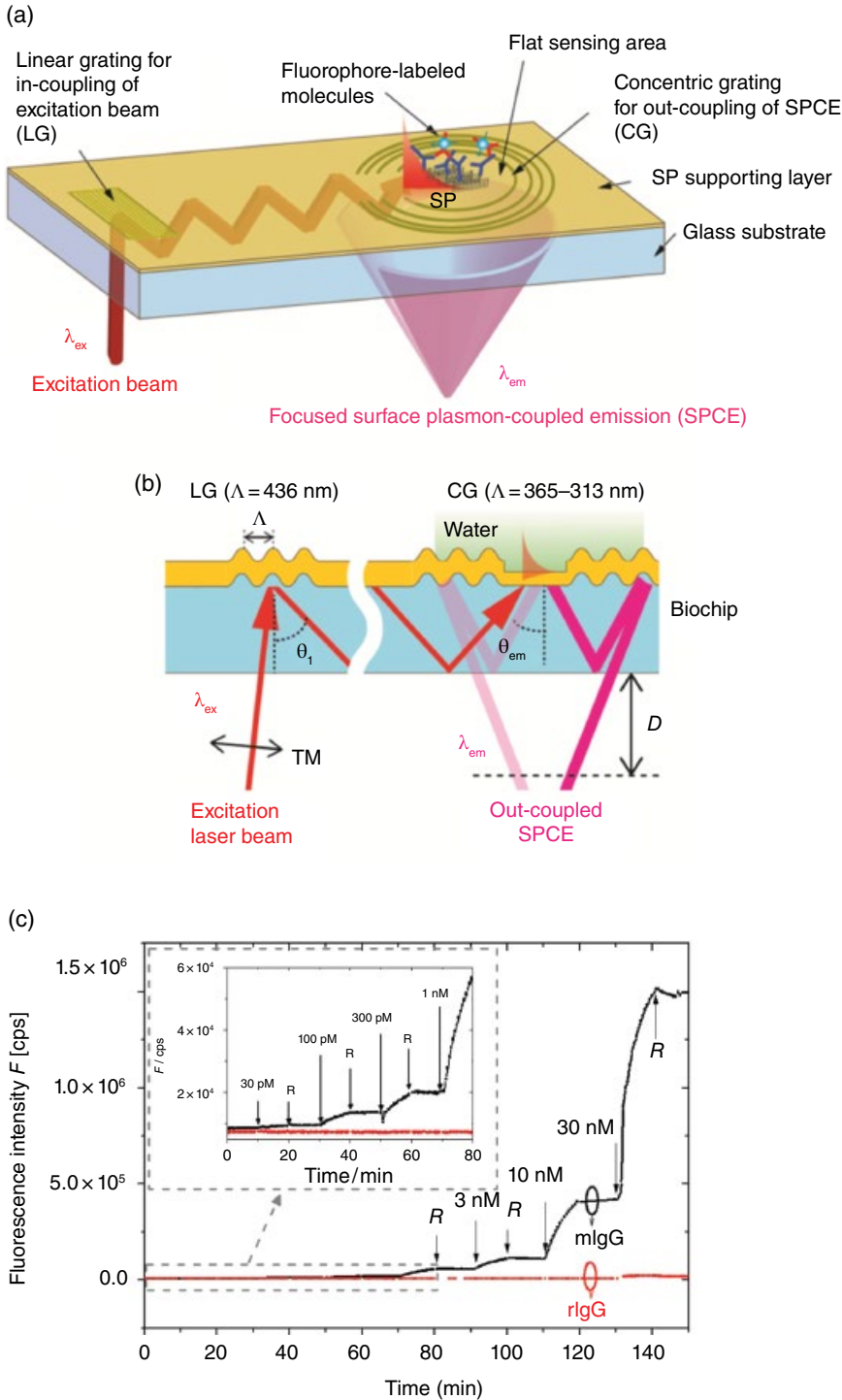


Figure 14.10 (a) Optical geometry for concentric grating-based out-coupling of SPCE from a sensor chip with reverse Kretschmann configuration and (b) its cross section. (c) Example of a model immunoassay experiment with a specific (mouse IgG: mlgG) and a control (rabbit IgG: rlgG) analytes present in analyzed samples. Toma *et al.* [27]. Reproduced with the permission of The Optical Society.

and thus enables improving the assay sensitivity and LOD. The amplification by propagating SPs can be carried out for optical sensors utilizing attenuated total internal reflection fluorescence (TIRF) as well

as epifluorescence configuration, and the enhancement factor of fluorescence signal intensity up to 10^2 can be reached. The plasmonically amplified fluorescence assays are particularly attractive for *in situ*

measurements and provide versatile platform where both excitation and collection of fluorescence light can be performed through a dielectric sensor chip [26], through a microfluidic system on the top of the sensor chip [28], or for the excitation and collecting from opposite sides is possible [19].

Acknowledgments

This work was partially supported by Austrian Science Fund (FWF) through the project ACTIPLAS (P244920-N20) and this project has received funding from the European Union's Horizon 2020 research and innovation programme under grant agreement no. 633937, project ULTRAPLACAD.

References

- Bally, M.; Halter, M.; Voros, J.; Grandin, H. M., Optical microarray biosensing techniques. *Surf. Interface Anal.* **2006**, *38* (11), 1442–1458.
- Seidel, M.; Niessner, R., Automated analytical microarrays: a critical review. *Anal. Bioanal. Chem.* **2008**, *391* (5), 1521–1544.
- Schuller, J. A.; Barnard, E. S.; Cai, W. S.; Jun, Y. C.; White, J. S.; Brongersma, M. L., Plasmonics for extreme light concentration and manipulation. *Nat. Mater.* **2010**, *9* (3), 193–204.
- Novotny, L.; van Hulst, N., Antennas for light. *Nat. Photonics* **2011**, *5* (2), 83–90.
- Attridge, J. W.; Daniels, P. B.; Deacon, J. K.; Robinson, G. A.; Davidson, G. P., Sensitivity enhancement of optical immunosensors by the use of a surface-plasmon resonance fluoroimmunoassay. *Biosens. Bioelectron.* **1991**, *6* (3), 201–214.
- Liebermann, T.; Knoll, W., Surface-plasmon field-enhanced fluorescence spectroscopy. *Colloids Surf. A Physicochem. Eng. Asp.* **2000**, *171* (1–3), 115–130.
- Barnes, W. L.; Preist, T. W.; Kitson, S. C.; Sambles, J. R., Physical origin of photonic energy gaps in the propagation of surface plasmons on gratings. *Phys. Rev. B* **1996**, *54* (9), 6227–6244.
- Sarid, D., Long-range surface-plasma waves on very thin metal-films. *Phys. Rev. Lett.* **1981**, *47* (26), 1927–1930.
- Chance, R. R.; Prock, A.; Silbey, R., *Adv. Chem. Phys.* **1978**, *37* (1), 1–65.
- Weber, W. H.; Eagen, C. F., Energy-transfer from an excited dye molecule to the surface-plasmons of an adjacent metal. *Opt. Lett.* **1979**, *4* (8), 236–238.
- Vareiro, M. L. M.; Liu, J.; Knoll, W.; Zak, K.; Williams, D.; Jenkins, A. T. A., Surface plasmon fluorescence measurements of human chorionic gonadotrophin: role of antibody orientation in obtaining enhanced sensitivity and limit of detection. *Anal. Chem.* **2005**, *77* (8), 2426–2431.
- Lakowicz, J. R.; Malicka, J.; Gryczynski, I.; Gryczynski, Z., Directional surface plasmon-coupled emission: a new method for high sensitivity detection. *Biochem. Biophys. Res. Commun.* **2003**, *307* (3), 435–439.
- Yuk, J. S.; Trnavsky, M.; McDonagh, C.; MacCraith, B. D., Surface plasmon-coupled emission (SPCE)-based immunoassay using a novel paraboloid array biochip. *Biosens. Bioelectron.* **2010**, *25* (6), 1344–1349.
- Knoll, W.; Philpott, M. R.; Swalen, J. D., Emission of light from Ag metal gratings coated with dye monolayer assemblies. *J. Chem. Phys.* **1981**, *75* (10), 4795–4799.
- Kitson, S. C.; Barnes, W. L.; Sambles, J. R., Photoluminescence from dye molecules on silver gratings. *Opt. Commun.* **1996**, *122* (4–6), 147–154.
- Toma, K.; Dostalek, J.; Knoll, W., Long range surface plasmon-coupled emission for biosensor applications. *Opt. Express* **2011**, *19* (12), 11090–11099.
- Soboleva, I. V.; Descrovi, E.; Summonte, C.; Fedyanin, A. A.; Giorgis, F., Fluorescence emission enhanced by surface electromagnetic waves on one-dimensional photonic crystals. *Appl. Phys. Lett.* **2009**, *94* (23), 231122.
- Zhang, W.; Ganesh, N.; Mathias, P. C.; Cunningham, B. T., Enhanced fluorescence on a photonic crystal surface incorporating nanorod structures. *Small* **2008**, *4* (12), 2199–2203.
- Toma, K.; Descrovi, E.; Toma, M.; Ballarini, M.; Mandracci, P.; Giorgis, F.; Mateescu, A.; Jonas, U.; Knoll, W.; Dostalek, J., Bloch surface wave-enhanced fluorescence biosensor. *Biosens. Bioelectron.* **2013**, *43*, 108–114.
- Toma, M.; Toma, K.; Adam, P.; Vala, M.; Homola, J.; Knoll, W.; Dostalek, J., Surface plasmon-coupled emission on plasmonic Bragg gratings. *Opt. Express* **2012**, *20* (13), 14042–14053.
- Bauch, M.; Hageneder, S.; Dostalek, J., Plasmonic amplification for bioassays with epi-fluorescence readout. *Opt. Express* **2014**, *22* (26), 32026–32038.
- Tawa, K.; Hori, H.; Kintaka, K.; Kiyosue, K.; Tatsu, Y.; Nishii, J., Optical microscopic observation of fluorescence enhanced by grating-coupled surface plasmon resonance. *Opt. Express* **2008**, *16* (13), 9781–9790.
- Bharadwaj, P.; Novotny, L., Spectral dependence of single molecule fluorescence enhancement. *Opt. Express* **2007**, *15* (21), 14266–14274.

- 24 Kinkhabwala, A.; Yu, Z. F.; Fan, S. H.; Avlasevich, Y.; Mullen, K.; Moerner, W. E., Large single-molecule fluorescence enhancements produced by a bowtie nanoantenna. *Nat. Photonics* **2009**, 3 (11), 654–657.
- 25 Gogalic, S.; Hageneder, S.; Ctorticka, C.; Bauch, M.; Khan, I.; Preininger, C.; Sauer, U.; Dostalek, J., Plasmonically Amplified Fluorescence Bioassay with Microarray Format. *Proc. SPIE* **2015**, 9506 (Optical Sensors 2015), 95060N.
- 26 Toma, K.; Adam, P.; Vala, M.; Homola, J.; Knoll, W.; Dostalek, J., Compact biochip for plasmon-enhanced fluorescence biosensor. *Opt. Express* **2013**, 21 (8), 10121–10132.
- 27 Toma, K.; Vala, M.; Adam, P.; Homola, J.; Knoll, W.; Dostalek, J., Compact surface plasmon-enhanced fluorescence biochip. *Opt. Express* **2013**, 21 (8), 10121–10132.
- 28 Hageneder, S.; Bauch, M.; Dostalek, J., Plasmonically amplified fluorescence bioassay - total internal reflection vs. epifluorescence geometry, *Talanta* 156–157, 225–231.